SDRP Journal of Nanotechnology & Material Science (ISSN: 2574-1888)

Synthesis and mechanical properties of bulk metallic nanoglasses: A brief review

DOI: 10.25177/JNMS.2.1.RA.560

Research

Received Date: 10th Aug 2019
Accepted Date: 15th Sep 2019
Published Date:20th Sep 2019

Yue Dong[a], Jian-Zhong Jiang[b], and Hans-Jörg Fecht[a]

[a] Institute of Functional Nanosystems, University of Ulm, Albert-Einstein Allee 47, 89081 Ulm, Germany

[b] International Center for New-Structured Materials, State Key Laboratory of Silicon Materials and School of Materials Science and Engineering, Zhejiang University, 310027 Hangzhou, P.R. China

CORRESPONDENCE AUTHOR

Yue Dong
Email: yue.dong@uni-ulm.de

CITATION

Yue Dong, Jian-Zhong Jiang, Hans-Jörg Fecht, Synthesis and mechanical properties of bulk metallic nanoglasses: A brief review(2019)SDRP Journal of Nanotechnology & Material Science 2(1) p:106-120

ABSTRACT

Metallic nanoglass is a newly developed metallic glass material exhibiting nanometer-sized glassy clusters interspersed with glass/glass interfaces. The glass/glass interfaces with greater free volume offer more shear transformation sites during plastic deformation while the relative denser nanometer-sized glassy clusters could effectively hinder shear band sliding, resulting in considerably improved mechanical properties in metallic glasses. This article reviews three synthesis methods for bulk metallic nanoglasses. The first method is inert gas condensation. The second method – with the appropriate morphology and distribution of the glass material – allows bulk metallic nanoglasses to be obtained using chemical methods initiated through phase separation. The third method includes the introduction of large numbers of shear bands with different orientations by using severe plastic deformation. The article concludes with a discussion of the mechanical properties of the different bulk metallic nanoglasses prepared using the various methods described.

Keywords: Bulk metallic nanoglasses; Nanometer-sized amorphous structures; Mechanical properties

1. INTRODUCTION

Metallic materials are traditionally considered crystalline in nature, possessing translational symmetry. Their constituent atoms are arranged in a regular and periodic manner in three dimensions. A revolution in this concept of metals was brought in 1960 that no crystalline structure was detected in a rapidly solidified Au-Si alloy, which is the discovery of metallic glass. In contrast to the crystalline metals, metallic glasses are amorphous materials formed at the glass transition temperature during continuous cooling of the liquid with cooling rates between 1 K/s to 10^{10} K/s depending on their compositions. Therefore, metallic glasses do not exhibit long range atomic order (like crystals and quasicrystals), but short to medium range order in the range of a few to a few tens of atoms [1-6].

Plastic deformation in crystalline alloys is basically achieved through the sliding/climbing of dislocations. Dislocations are crystallographic defects or irregularity within a crystal structure which can move by breaking the atoms bonds from one of the surrounding planes and rebonding with the atoms at the terminating edge. During cold-working, the dislocation density increases. The consequent increasing overlap between the strain fields of adjacent dislocations gradually increases the resistance to further dislocation motion, resulting in the work-hardening effect. Work-hardening makes the delocalized plastic strain spread out across the entire sample relatively easily. However, the deformation mechanism in metallic glasses is completely different [7]. Because there is no dislocation in amorphous structures, plastic deformation in metallic glasses can only proceed by way of atomic jumps in localized regions known as shear transformation zones (STZs), which involve in a group of atoms with much larger atomic displacements than surrounding matrix, and can rearrange spontaneously and cooperatively to accommodate the applied shear strain. These STZs further form a shear band, which is a narrow region (approximate 10-100 nm in thickness) of intense shearing strain [8]. Due to this special plastic deformation mechanism, most metallic glasses are very strong with the yield strength even exceeding 3 GPa in some metal–metalloid systems. While, this inhomogeneous deformation also results in very limited plastic stain. In plastic deformation, dilatation occurs in shear bands through the coalescence of free volume, something which can lead to the formation of voids and work-softening. Further increases in the degree of deformation exceed the offset limit of a shear band and crack will be formed. Generally speaking, for glasses the deformation energy release is concentrated only in a small localized region, the crack will be unstable and propagates quickly. Consequently, most glasses tend to be rather brittle materials [9,10].

The application range of crystalline materials is much wider than that of amorphous materials. Although glasses have been in use for thousands of years, their applications are mostly restricted to windows, lenses and optical fibers [11]. The main reason is that the microstructure of crystalline materials can be modified using various methods to control their properties. In order to make the metallic glasses microstructure modification possible and improve their mechanical properties (especially their ductility), the principle of nanoglasses has recently been proposed. The idea is to generate metallic glasses with glass/glass interfaces between adjacent regions as controllable defects [12,13], as shown in Figure 1 [2]. Similar to the multitude of boundaries in nano-crystalline materials, one way of introducing a high density of incoherent interfaces is by consolidating nanometer-sized clusters [14,15]. This newly-developed materials – nanoglasses – also have the following features which are beneficial to mechanical properties [16,17]: (1) Because of the enhanced atomic misfit, increased free volume in the glass/glass boundaries can offer more STZs and shear band initiation sites, making the plastic deformation homogeneous. (2) The propagation of shear bands can be hindered by the relative higher density of glassy clusters. The shear bands cannot slide unrestricted, resulting in a serrated shear and improving ductility [18].

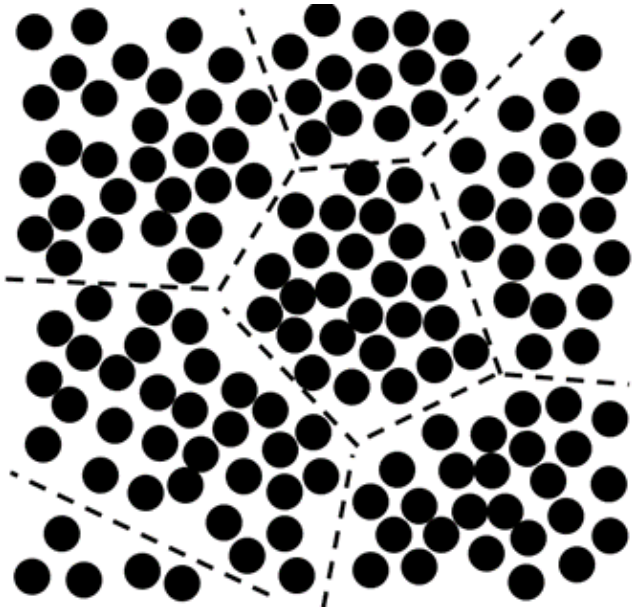

Figure 1. Schematic diagram of nanoglass structure consisting of glassy clusters and glass/glass boundaries.

2. Bulk metallic nanoglasses synthesized by inert gas condensation

During inert gas (e.g. Helium) condensation process, nanometer-sized glassy clusters are first evaporated from the target material into the inert gas atmosphere; then they consolidate on the surface of a rotating liquid nitrogen-cooled cylinder. Nanometer-sized glassy powders can be obtained by stripping the condensed nanometer-sized glassy clusters off the substrate. It is followed by the consolidation process, containing two steps: First, the powders are preconsolidated in an ultra-high vacuum system. The resulting sample is shaped like a disc (e.g., about 0.5 mm in thickness and about 5 mm in diameter). Second, this disc is compacted under high pressure (up to 5 GPa) [19,20]. To avoid oxidation, the high pressure consolidation process should be an in-situ procedure using inert gas condensation, as shown in Figure 2. Au-La, Fe-Si, Ni-Ti, and Sc-Fe bulk metallic nanoglasses can be prepared by inert gas condensation method [13,18,21,22].

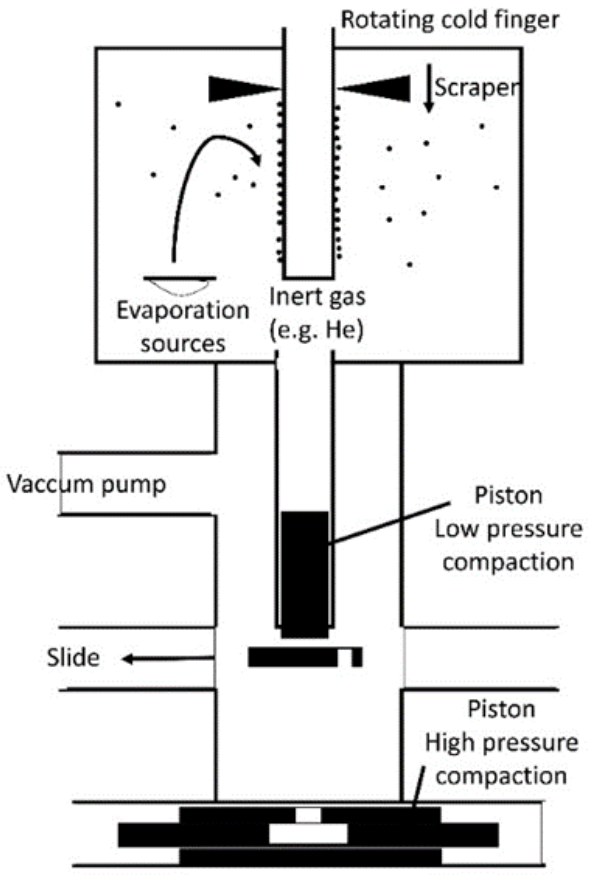

Figure 2. Production of bulk metallic nanoglasses using the consolidation of nanometer-sized glassy clusters generated by inert gas condensation [11,12].

Inert gas condensation prepared $Sc_{75}Fe_{25}$ bulk metallic nanoglass has high number of interfaces between the nano-scaled clusters The enhancement of free volume in bulk metallic nanoglasses, compared with solidification prepared metallic glasses with the same compositions, is confirmed by positron annihilation analysis [20,23]. Compression tests in Figure 3, performed on this $Sc_{75}Fe_{25}$ bulk metallic nanoglass and melt-quenched ribbons [20], reveal that the glassy ribbon exhibits brittle fracture at a stress of 1900 and 2200 MPa for the as-prepared and annealed states, respectively. The $Sc_{75}Fe_{25}$ bulk metallic nanoglass in as-consolidated state yields at a lower stress (1250 MPa). After the yield point, the bulk metallic nanoglass shows nonlinear plastic flow, i.e., a region of strain-hardening, followed by a fracture stress of 1950 MPa. Annealing is known to result in the embrittlement of metallic glasses because of the free volume annihilation during structural relaxation. Howev-

er, owing to the existence of abundant glass/glass interfaces which promote a high number of embryonic shear bands, bulk metallic nanoglass retains still a remarkable compressive plasticity with a slightly increased yield, even though annealed for 2 h at 200°C.

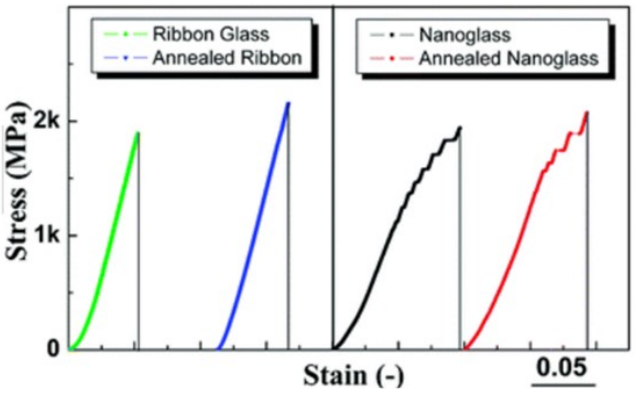

Figure 3. Stress−strain curves of $Sc_{75}Fe_{25}$ ribbon glasses and bulk metallic nanoglasses for as-prepared and annealed states prepared by inert gas condensation [20]. (Reprinted from Ref. [20]. Copyright © 2012 Nano Letters)

3. Bulk metallic nanoglasses synthesized by chemical phase separation

3.1. Structure of phase-separated bulk metallic nanoglasses

Chemical phase separation is a method developed for synthesis of amorphous composite materials. Its purpose is to introduce small amounts of elements into a metallic glass system, which has a positive enthalpy of mixing with another element in the matrix [24,25]. If the composition is designed carefully, this method can also be used to synthesize bulk metallic nanoglasses. Only a few works about phase separated bulk metallic nanoglasses have been published, one example of which is bulk metallic glass with the composition $Cu_{47.2}Zr_{46.5}Al_{5.5}Nb_{0.8}$ [26]. The bulk metallic nanoglass structure in the TEM picture (Figure 4) has dark Cu/Al-rich glassy clusters and bright Zr/Nb-rich glass/glass interfaces.

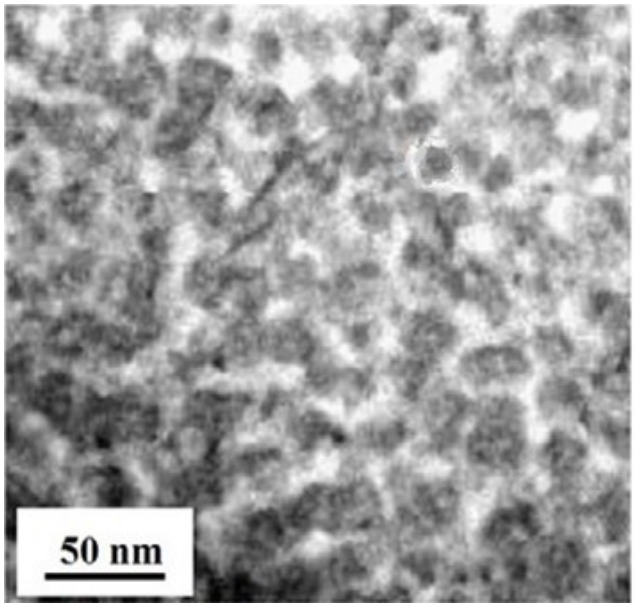

Figure 4. STEM-BF image showing the structure in phase-separated bulk metallic nanoglass of as-cast $Cu_{47.2}Zr_{46.5}Al_{5.5}Nb_{0.8}$ [26]. (Reprinted from Ref. [26]. Copyright © 2014 Scripta Materialia)

Another piece of systematic research has been conducted on the composition design and structure characterization of $Zr_{64-x}Ni_{10}Al_7Cu_{19}Co_x$ (x = 0–16) metallic glasses [27]. Cobalt and copper have positive enthalpy of mixing (6 kJ/mol), while highly negative enthalpy of mixing occurs for cobalt and zirconium (−41 kJ/mol) [28]. The XRD patterns of as-cast $Zr_{64-x}Ni_{10}Al_7Cu_{19}Co_x$ (x = 0–16 at.%) samples (2 mm rods) in Figure 5 show that samples with a Co content above 8.3 at.% are partial crystallized. When the Co content is below 8.3 at.%, the samples are fully amorphous. The position of the maximum scattering intensity of the XRD curves shift right to a higher 2θ value as the Co content increases from 36.58° for $Zr_{64}Ni_{10}Al_7Cu_{19}$ to 37.12° for $Zr_{55.7}Ni_{10}Al_7Cu_{19}Co_{8.3}$, indicating a contraction of the average atomic bond, while the mass density measured by Archimedes' method increases from 6.796 g/cm^3 for $Zr_{64}Ni_{10}Al_7Cu_{19}$ to 6.888 g/cm^3 for $Zr_{55.7}Ni_{10}Al_7Cu_{19}Co_{8.3}$.

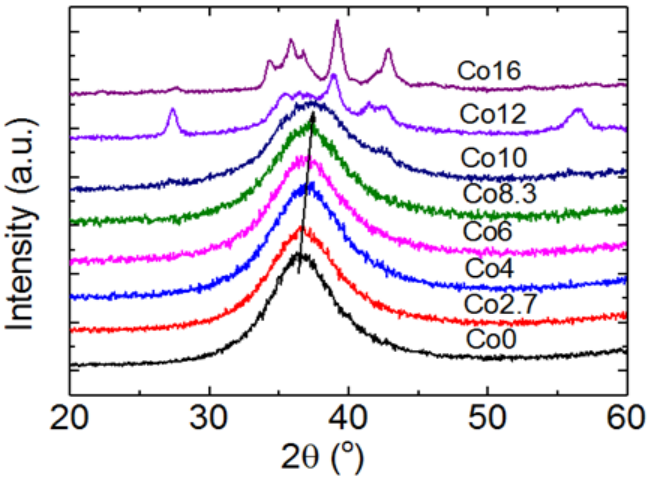

Figure 5. XRD patterns of as-cast 2 mm-rod samples with composition $Zr_{64-x}Ni_{10}Al_7Cu_{19}Co_x$ (x = 0–16 at.%). (Reprinted from Ref. [27]. Copyright © 2017 Scripta Materialia)

XRD is a powerful tool for structure analysis on crystalline materials. But for the glass or nanoglass, little information can be obtained from the patterns because of the absence of diffraction peaks. TEM analyses can be used for the intuitive observation of the size, shape and distribution of the various phases. The images show obvious structural differences (Figure 6). The structure of as-cast $Zr_{64}Ni_{10}Al_7Cu_{19}$ 2 mm-rod bulk metallic glass is relatively homogeneous under TEM. However, nanometer-scale amorphous clusters are clearly detectable in the as-cast $Zr_{55.7}Ni_{10}Al_7Cu_{19}Co_{8.3}$ 2 mm-rod sample. The electron diffraction patterns show the same results as XRD; both samples have a fully amorphous structure [27]. Thus, we assign the as-cast $Zr_{55.7}Ni_{10}Al_7Cu_{19}Co_{8.3}$ 2 mm-rod sample as a bulk metallic nanoglass.

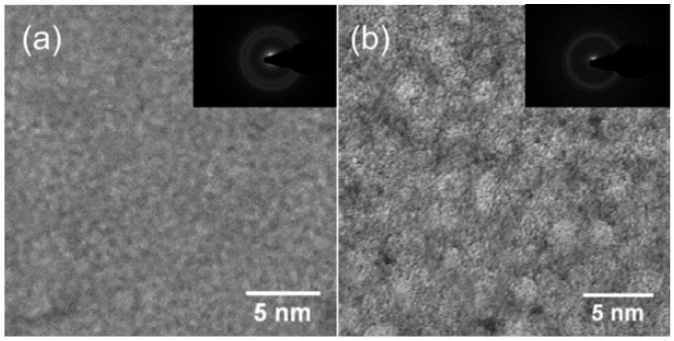

Figure 6. TEM images of (a) $Zr_{64}Ni_{10}Al_7Cu_{19}$ bulk metallic glass and (b) $Zr_{55.7}Ni_{10}Al_7Cu_{19}Co_{8.3}$ bulk metallic nanoglass.

Synchrotron radiation XRD with a shorter wavelength (0.124 Å) can be used to characterize the finer atomic structure of bulk metallic glasses. The structure factors S(Q) can be obtained from the diffraction intensity data. All of the $Zr_{64-x}Ni_{10}Al_7Cu_{19}Co_x$ (x=0–8.3 at.%) samples exhibit similar S(Q) in Figure 7 and pair distribution G(r) in Figure 10. As shown in the magnified image of the first peaks on S(Q) (Figure 7 (b)), increased Co content leads to an increase in the first peak position and a decrease in the first peak amplitude. As shown in the magnified image of the first peaks on G(r) (Figure 8 (b)), increased Co content leads to a decrease in the first peak amplitude and an increase in the height of its left-hand shoulder (r ≈ 2.72 Å). These results indicate that the addition of Co into this bulk metallic glass leads to a rearrangement of the atomic packing and the formation of a new topological structure with shorter atomic bonds, resulting in reduced average atomic distance.

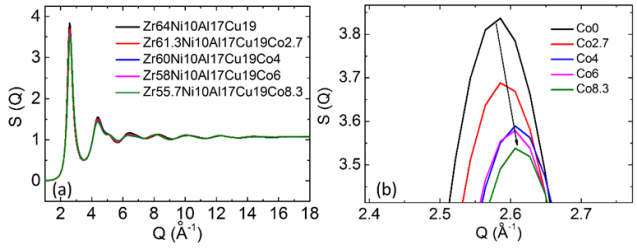

Figure7. (a) Structure factors of as-cast $Zr_{64-x}Ni_{10}Al_7Cu_{19}Co_x$ (x = 0–8.3 at.%) bulk metallic glasses and (b) magnification of the first peaks on their structure factors. (Reprinted from Ref. [27]. Copyright © 2017 Scripta Materialia)

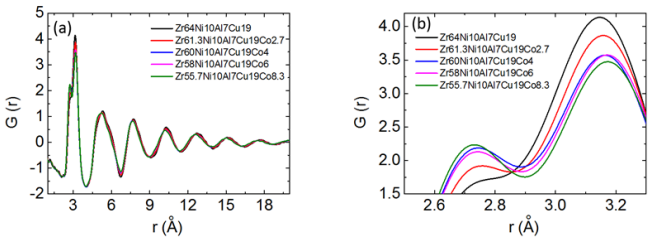

Figure 8. (a) Pair distribution functions (PDFs) and (b) magnification of the first peaks on PDFs of $Zr_{64-x}Ni_{10}Al_7Cu_{19}Co_x$ (x = 0–8.3 at.%) bulk metallic glass samples. (Reprinted from Ref. [27]. Copyright © 2017 Scripta Materialia)

Extended X-ray absorption fine structure (EXAFS) analyses are a useful tool for investigating the structure of nanoglass. It can provide information about the chemical coordination environment of the central absorbing element, which can be used to further analyze the topological structure of materials [29]. The Co-K edge EXAFS results (Figure 9 (a)) reveal no obvious difference between $Zr_{60}Ni_{10}Al_7Cu_{19}Co_4$ and $Zr_{55.7}Ni_{10}Al_7Cu_{19}Co_{8.3}$ bulk metallic glasses. The atomic environment surrounding Co is not influenced by changing the Co content. This means that the newly-formed topological structure does not change with different Co contents. On the Zr-K edge EXAFS results (Figure 9 (b)), the height of the Zr-Zr bond peak (2.90 Å) reduces when the Co content is increased. Meanwhile, the peak height of Zr-Ni, Zr-Cu, and/or Zr-Co bonds increases (their bond lengths are similar and cannot be distinguished from each other on the curves). Furthermore, the maximum point of this peak (Zr-Ni, Zr-Cu, or/and Zr-Co bonds) shifts left from 2.48 Å to a smaller value of 2.41 Å, indicating the reduced atomic bond length. This means that, with the formation of a new topological structure, Zr-Zr and Zr-Cu bonds are replaced by the shorter and stronger Zr-Co bonds, resulting in a reduced average atomic distance in the $Zr_{64-x}Ni_{10}Al_7Cu_{19}Co_x$ (x = 0–8.3 at.%) BMGs [27].

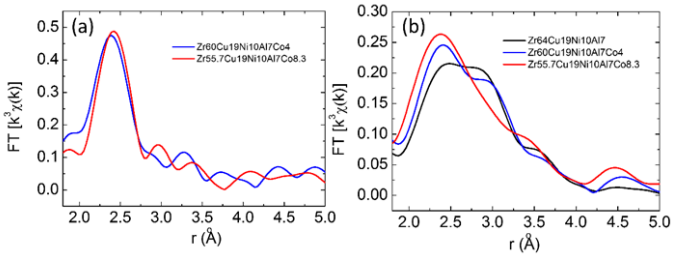

Figure 9. EXAFS analysis of (a) Co K-edge data and (b) Zr K-edge data of selected $Zr_{64-x}Ni_{10}Al_7Cu_{19}Co_x$ (x = 0, 4 and 8.3 at.%) bulk metallic glasses. (Reprinted from Ref. [27]. Copyright © 2017 Scripta Materialia)

3.2. Mechanical properties of phase-separated bulk metallic nanoglasses

Figure 10 shows the compressive stress–strain curve of the phase-separated $Cu_{47.2}Zr_{46.5}Al_{5.5}Nb_{0.8}$ bulk metallic nanoglass. It has an elastic strain limit of 1.95% and a yield stress of 1678 MPa. Work hardening can be observed at the beginning of plastic deformation. The plastic strain is as high as 16.3%. A large number of shear bands are distributed relatively homogeneously on the surface of deformed sample, intersecting and interconnecting with each other [26]. This confirms that, in the nanoglass structure, the interfaces offer more shear band initiation sites. And the blocking of shear band propagation by glassy clusters leads to shear band proliferation, resulting in a high level of plastic strain.

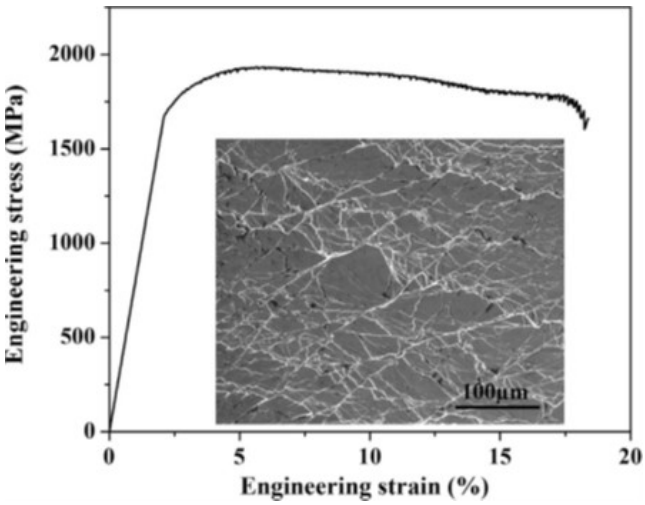

Figure10. Compressive stress–strain curve of $Cu_{47.2}Zr_{46.5}Al_{5.5}Nb_{0.8}$ bulk metallic nanoglass. Inset: SEM image showing shear bands on the surface of a deformed sample [26]. (Reprinted from Ref. [26]. Copyright © 2014 Scripta Materialia)

The mechanical properties of $Zr_{64-x}Ni_{10}Al_7Cu_{19}Co_x$ series bulk metallic glasses were also investigated [27]. Table 1 shows their Young's modulus and hardness measured using the ultrasound pulse-echo technique and nanoindentation. It shows that the Young's modulus and hardness of these bulk metallic glasses both increase monotonically with the Co content. This could be due to the replacement of more Zr-Zr and Zr-Cu bonds by Zr-Co bonds. As discussed above, Zr-Co bonds are shorter and stronger, leading to the increased Young's modulus and hardness.

Table1. Young's modulus and hardness of $Zr_{64-x}Ni_{10}Al_7Cu_{19}Co_x$ (x = 0–8.3 at.%) bulk metallic glasses.

Co (at.%)	Young's modulus (GPa)	Hardness (GPa)
0	74.9	5.3
2.7	78.8	5.5
4	83.6	5.9
6	81.1	5.9
8.3	84.4	6.2

Figure 11 shows the compressive stress–strain curves of $Zr_{64-x}Ni_{10}Al_7Cu_{19}Co_x$ bulk metallic glasses and bulk metallic nanoglass. The Young's modulus of both samples is consistent with the results measured using the ultrasound pulse-echo technique. The maximum elastic strain increases dramatically from 1.8% to 2.6% because of the stronger atomic bonds and the blocking effect of the glassy clusters on shear band sliding. The ductility of $Zr_{55.7}Ni_{10}Al_7Cu_{19}Co_{8.3}$ bulk metallic nanoglass improves compared with the relatively homogeneous bulk metallic glass, with its plastic strain reaching approximately 4%.

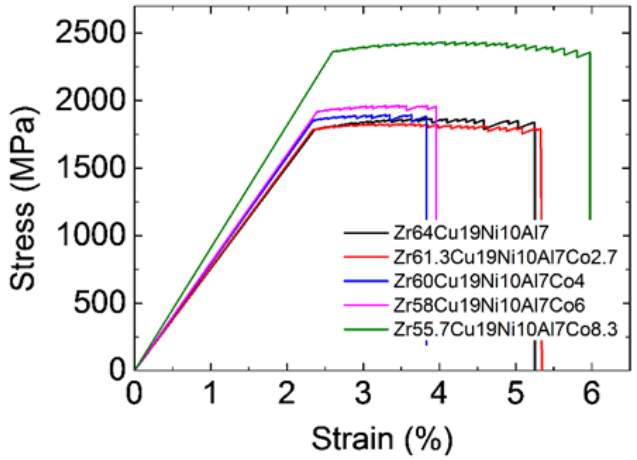

Figure 11. Compressive stress–strain curves of $Zr_{64-x}Ni_{10}Al_7Cu_{19}Co_x$ (x = 0–8.3 at.%) bulk metallic glasses and bulk metallic nanoglass. (Reprinted from Ref. [27]. Copyright © 2017 Scripta Materialia)

Shear band intersections can be observed on the surface of deformed $Zr_{55.7}Ni_{10}Al_7Cu_{19}Co_{8.3}$ bulk metallic nanoglass (Figure 12). The interfaces in the bulk metallic nanoglass with more free volume lead to more shear bands forming during compression, resulting in more homogeneous deformation. The propagation directions of these shear bands are altered by the denser glassy clusters [30], as confirmed by the observation of the shear band intersections, leading to improved plasticity and strength.

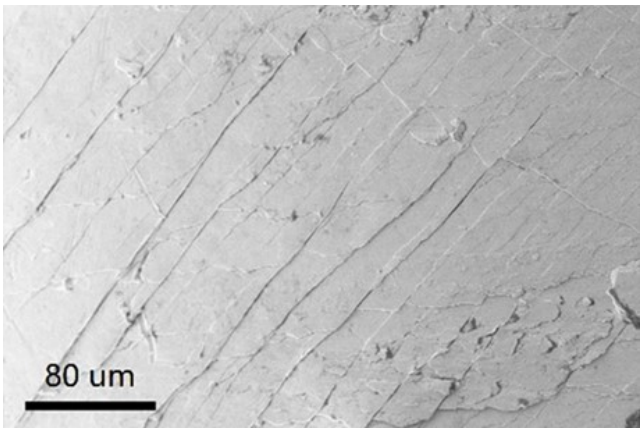

Figure 12. SEM image of the surface of the deformed $Zr_{55.7}Ni_{10}Al_7Cu_{19}Co_{8.3}$ bulk metallic nanoglass (green curve in Figure 11). (Reprinted from Ref. [27]. Copyright © 2017 Scripta Materialia)

4. Bulk metallic nanoglasses synthesized by severe plastic deformation

4.1.Shear bands

Introducing shear bands could be a possible method for achieving nanoglass synthesis. If so, then shear bands and the glass/glass interfaces should have a similar size and structure. Some prior research has investigated the thickness of shear bands. HRTEM images show that the shear bands in ball-milled $Zr_{70}Cu_{20}Ni_{10}$ metallic glass have a width of 10-20 nm [31]. The observation of shear bands using electron microscopes is sometimes not unproblematic. Theoretical calculations were therefore also used to detect the thickness of shear bands. Molecular dynamics simulations [32,33] showed similar results, namely that the thickness of shear bands was around 10 nm. It is worth noting that in some research, such as indentation [34] and fusible-coating analysis [35], the shear bands were measurable in micrometers. The reason is that shear bands have a core region with rearranged atoms, with a stress/heating field surrounding it. The real thickness of shear bands is actually the core region, which is about 10 nm. The size

of the glass/glass interfaces in nanoglass is also around 10 nm; these usually include tens to hundreds of atoms.

Another structural feature of these interfaces in nanoglass is their enhanced free volume due to atomic misfit. The increased free volume in shear bands has been proven by experiments and simulation work. 1-2% volume expansion is observed in shear bands [36,37]. Enthalpy increase [38] and tracer measurements [39] also confirmed the change in free volume. Simulation work [40] showed that free volume in shear bands is unstable in thermodynamics and that it tends to gather in one place.

In summary, shear bands have a similar feature to the glass/glass interfaces, including their nano-scaled size and increased free volume. This again confirms that introducing shear bands could be an effective method for achieving nanoglass synthesis. Having said this, in order to get the glassy clusters, it is necessary to have a high number density of shear bands and network structure.

4.2. Bulk metallic nanoglasses prepared by high pressure torsion

Plastic deformation is a common used method for shear bands introduction in metallic glasses. While, the network structure is difficult to form by conventional plastic deformation treatments such as cold-rolling [7]. High pressure torsion (HPT) is a newly-developed severe plastic deformation method for the structural modification of materials. It was primarily intended as a way of investigating the deformation of different elements under high pressure [41]. Compared with other methods, HPT is more efficient for introducing high angle grain boundaries into crystalline metals. It is therefore fair to expect the formation of large number of shear bands and network structure in the HPT-treated metallic glasses. Synchrotron radiation XRD measurements show that, after HPT treatment, the atomic order was reduced and the free volume was increased in Au-based [42] and Zr-based [43] bulk metallic glasses. It can lead to improved plasticity by reducing the velocity of shear band sliding, something which is proven by nanoindentation analysis [44]. HPT-treated $Zr_{65}Al_{7.5}Ni_{10}Cu_{12.5}Pd_5$ metallic glass exhibits work-hardening behavior and enhanced ductility during tension [45]. These structural changes are also accompanied by a rise in residual stress from the inhomogeneous plastic flow with a strain gradient. The tensile stress in the sample center results in a reduction in hardness, and the compressive stress leads to hardening on the edge of the HPT-treated metallic glasses [46]. Nanocrystallization can take place during HPT in metallic glasses with low thermal stability, such as $Nd_{11.8}Fe_{82.3}B_{5.9}$, $Ti_{50}Ni_{25}Cu_{25}$ and $Cu_{60}Zr_{30}Ti_{10}$. The reasons for this are the heating effect and topological structure change in the materials during severe plastic deformation [47,48].

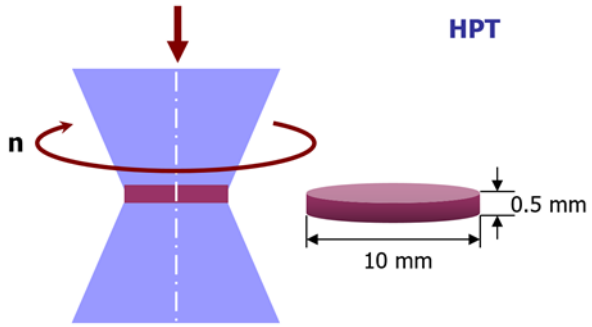

Figure 13. Schematic diagram of High Pressure Torsion (HPT).

Heterogeneous plastic deformation during HPT makes the formation of shear band networks possible (Figure 14) [2,42]. Micro-region synchrotron radiation XRD [49] shows that HPT-treated CuZr-based bulk metallic glass has structural and mechanical heterogeneities on the submicron scale.

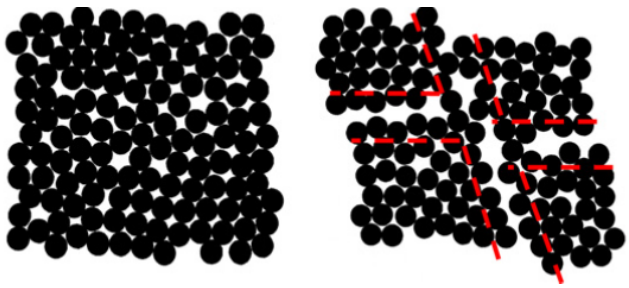

Figure 14. Schematic diagram of the formation of nanoglass by severe plastic deformation [2,42]. (Reprinted from Ref. [42]. Copyright © 2011 Scripta Materialia)

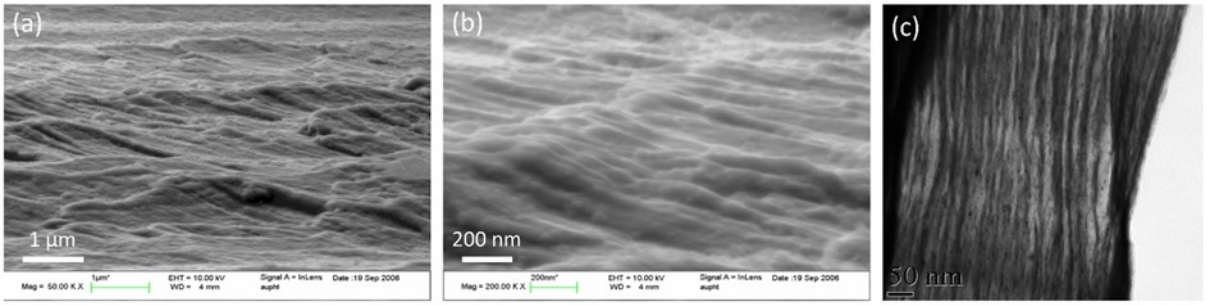

Figure 15. (a) (b) SEM and (c) TEM images of a cross-section through the $Au_{49}Ag_{5.5}Pd_{2.3}Cu_{26.9}Si_{16.3}$ bulk metallic glasses after HPT [42]. (Reprinted from Ref. [42]. Copyright © 2011 Scripta Materialia)

Published research works on bulk metallic nanoglasses formed by severe plastic deformation are not many. One study did examine HPT-treated $Au_{49}Ag_{5.5}P_{d2.3}Cu_{26.9}Si_{16.3}$ bulk metallic glass [42]. It was possible to obtain a bulk metallic nanoglass structure on this glass type. Figure 15 shows SEM and TEM micrographs for the cross-section of the HPT-treated sample. It exhibits a modulated structural feature with a spacing of about 50–100 nm. Although the morphology of the glassy clusters is not like the as-cast crystalline grains as we expected, the shear band network is obviously formed with a large number of glass/glass interfaces. The increased free volume is confirmed by their DSC results and structure factors, which always yield better ductility. The size and shape of the glassy clusters can be affected by the HPT pressure, rotation speed, strain, temperature and so on. This structure can therefore be further modified by changing the HPT treatment parameters to meet different requirements.

4.3. Structural modification of phase-separated bulk metallic nanoglasses by severe plastic deformation

Some interesting research has been undertaken on the effects of HPT on bulk metallic nanoglass. As discussed above, $Zr_{55.7}Ni_{10}Al_7Cu_{19}Co_{8.3}$ bulk metallic glass has a phase-separated nanoglass structure. HPT can further modify this structure [50]. Figure 16 shows the TEM image of $Zr_{55.7}Ni_{10}Al_7Cu_{19}Co_{8.3}$ bulk metallic nanoglass after HPT treatment (2 rotations) [50]. The $Zr_{55.7}Ni_{10}Al_7Cu_{19}Co_{8.3}$ bulk metallic nanoglass has low thermal stability because of the positive mixing enthalpy between Co and Cu, resulting in nano-scaled crystallization during this severe plastic deformation. The nanometer crystalline particles appear as bright points on the dark field image. HPT-introduced shear bands also appear as dark lines due to their looser atomic structure. It should be noted that more nanocrystalline particles are found along shear bands compared to the matrix, because of the high degree of plastic deformation. Figure 17 shows the tension stress-strain curves of the as-cast and HPT treated $Zr_{55.7}Ni_{10}Al_7Cu_{19}Co_{8.3}$ bulk metallic nanoglasses. As-cast $Zr_{55.7}Ni_{10}Al_7Cu_{19}Co_{8.3}$ shows almost no plastic strain in tension. After HPT, its tensile ductility is improved significantly, reaching 1%. Plastic strain of 0.9% is a high value for metallic glasses under tension with a slow strain rate and at room temperature.

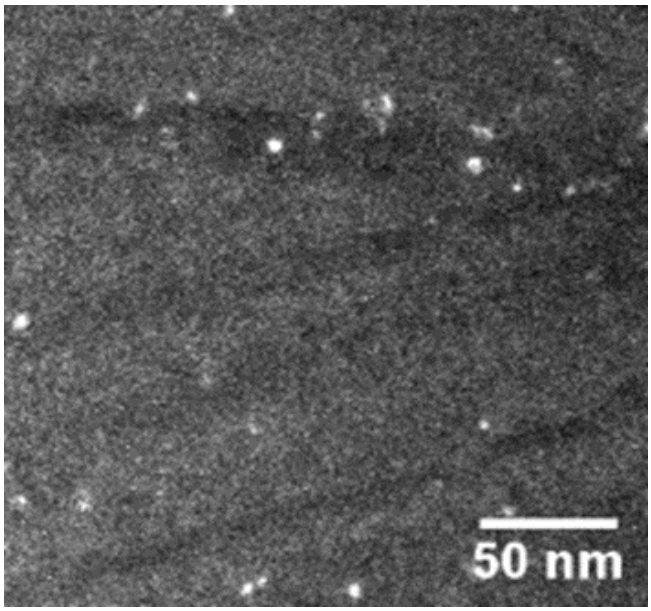

Figure 16. Dark-field image of HPT-treated (N=2) $Zr_{55.7}Ni_{10}Al_7Cu_{19}Co_{8.3}$ bulk metallic nanoglass [50]. (Reprinted from Ref. [50]. Copyright © 2019 Materials)

Table 2. Tensile yield stress, glass transition temperature T_g, position of the first maximum on structure factor curves, tensile plastic strain and enthalpy of relaxation of $Zr_{64}Ni_{10}Al_7Cu_{19}$ bulk metallic glass and $Zr_{55.7}Ni_{10}Al_7Cu_{19}Co_{8.3}$ bulk metallic nanoglass samples before and after HPT processes (N=2, 5, 10 and 20).

	$Zr_{64}Ni_{10}Al_7Cu_{19}$ bulk metallic glass					$Zr_{55.7}Ni_{10}Al_7Cu_{19}Co_{8.3}$ bulk metallic nanoglass				
	As cast	N=2	N=5	N=10	N=20	As cast	N=2	N=5	N=10	N=20
Tensile yield stress (MPa)	1265 ±30	1280 ±30	1270 ±30	1285 ±30	1270 ±30	1490 ±30	1540 ±30	1530 ±30	1520 ±30	1535 ±30
T_g (K)	648 ±3	649 ±3	647 ±3	650 ±3	648 ±3	674 ±3	676 ±3	673 ±3	675 ±3	675 ±3
Position of first maximum ($Å^{-1}$)	2.587 ±0.001	2.584 ±0.001	-	-	2.583 ±0.001	2.620 ±0.001	2.614 ±0.001	-	-	2.617 ±0.001
Tensile plastic strain (%)	0	0.5 ±0.1	0.2 ±0.1	0.2 ±0.1	0.2 ±0.1	0.1 ±0.1	0.9 ±0.1	0.2 ±0.1	0.1 ±0.1	0.2 ±0.1
Enthalpy of relaxation (J/g)	-4.9 ±0.5	-8.4 ±0.5	-7.1 ±0.5	-7.5 ±0.5	-7.3 ±0.5	-10.9 ±0.5	-17.3 ±0.5	-6.0 ±0.5	-6.2 ±0.5	-6.3 ±0.5

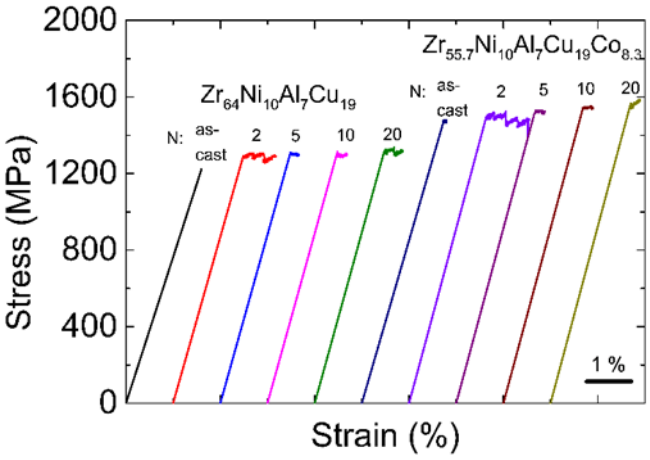

Figure17. Tensile stress–strain curves of $Zr_{64}Ni_{10}Al_7Cu_{19}$ metallic glasses and $Zr_{55.7}Ni_{10}Al_7Cu_{19}Co_{8.3}$ bulk metallic nanoglasses before and after HPT process. (Reprinted from Ref. [50]. Copyright © 2019 Materials)

Table 2 lists the tensile yield stress, glass transition temperature T_g and position of the first scattering intensity maximum on structure factor curves of $Zr_{64}Ni_{10}Al_7Cu_{19}$ bulk metallic glass and $Zr_{55.7}Ni_{10}Al_7Cu_{19}Co_{8.3}$ bulk metallic nanoglass samples before and after HPT processes (N=2, 5, 10 and 20). It can be seen that the introduction of Co leads to right-shift of the first maximum on structure factor (also shown in Figure 18), indicating a reduced average atomic distance. The reason is the formed shorter and stronger Zr-Co bond. Because of these stronger atomic bonds, both tensile yield stress and T_g increase with the addition of Co. HPT treatment has little effect on them.

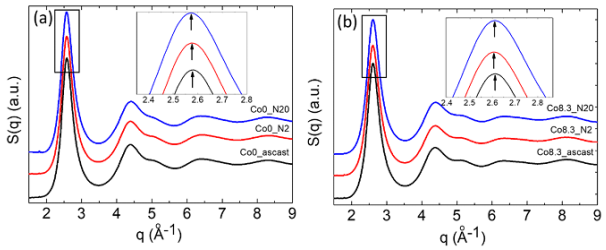

Figure 18. Structure factor curves of $Zr_{64}Ni_{10}Al_7Cu_{19}$ bulk metallic glass and $Zr_{55.7}Ni_{10}Al_7Cu_{19}Co_{8.3}$ bulk metallic nanoglass samples before and after HPT processes (N=2, 5, 10 and 20). (Reprinted from Ref. [50]. Copyright © 2019 Materials)

Tensile plastic strain and enthalpy of relaxation of $Zr_{64}Ni_{10}Al_7Cu_{19}$ bulk metallic glass and $Zr_{55.7}Ni_{10}Al_7Cu_{19}Co_{8.3}$ bulk metallic nanoglass samples before and after HPT processes are also summarized in Table 2. It can be seen that bulk metallic nanoglass has larger relaxation enthalpy compared with the bulk metallic glass. This relaxation enthalpy

change is analyzed by differential scan calorimetry (DSC) as shown in Figure 19. Two rotations HPT can further increase the relaxation enthalpy by the introduction of shear bands. Larger relaxation enthalpy is usually related to higher free volume content which can result in more homogeneous plastic deformation and better ductility. By addition of 8.3 % Co and 2 rotations HPT, a considerable increase of tensile plasticity strain from 0 % to about 1 % takes place. During in-situ tensile testing, SEM can be used to observe the shear bands' behavior and cracks propagation on the as-cast and HPT-treated $Zr_{55.7}Ni_{10}Al_7Cu_{19}Co_{8.3}$ bulk metallic nanoglasses. The images in Figure 20 show the surfaces of samples under yielding load. Two to three shear band intersections can be detected on the as-cast bulk metallic nanoglass. However, on the HPT-treated sample, multiple shear bands interact with each other, snaking across the surface [50].

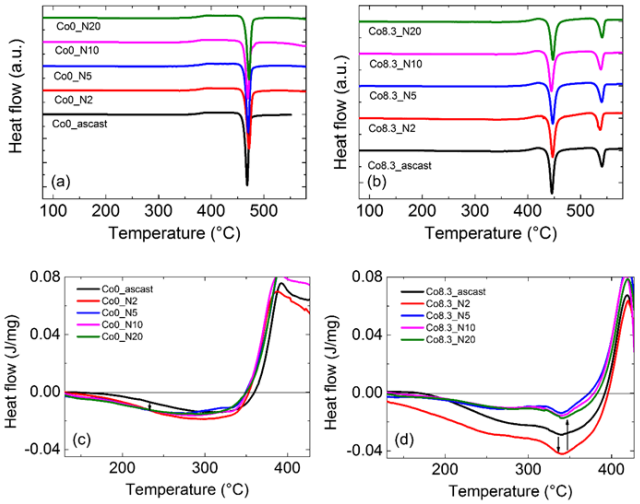

Figure 19. Differential scan calorimetry (DSC) curves of as-cast and HPT-treated (a) $Zr_{64}Ni_{10}Al_7Cu_{19}$ and (b) $Zr_{55.7}Ni_{10}Al_7Cu_{19}Co_{8.3}$ BMGs with different HPT rotation numbers. Relaxation energy release below T_g of as-cast and HPT-treated (c) $Zr_{64}Ni_{10}Al_7Cu_{19}$ and (d) $Zr_{55.7}Ni_{10}Al_7Cu_{19}Co_{8.3}$ BMGs with different HPT rotation numbers. (Reprinted from Ref. [50]. Copyright © 2019 Materials)

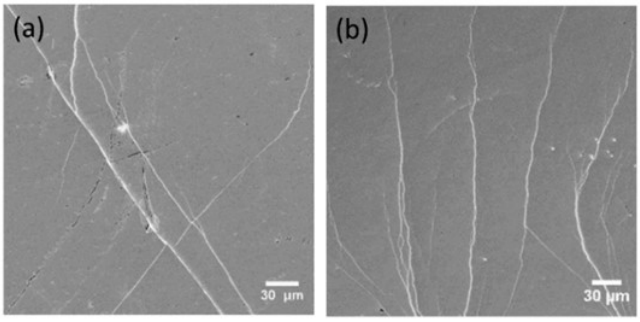

Figure 20. Densest areas of shear bands on the surface of the $Zr_{55.7}Ni_{10}Al_7Cu_{19}Co_{8.3}$ sample (a) as-cast, (b) HPT-treated [50]. (Reprinted from Ref. [50]. Copyright © 2019 Materials)

Finite element analyses of the tensile behaviors of metallic glasses and nanoglasses have also been undertaken [21]. It shows that heterogeneous free volume dispersion can improve the sample's plasticity effectively. The HPT-treated (N=2) $Zr_{55.7}Ni_{10}Al_7Cu_{19}Co_{8.3}$ bulk metallic nanoglass just has a similar structure that free volume content is high in the introduced shear bands (1-2% volume expansion compared with matrix) and low in the formed nano-crystalline particles. The simulation shows that, during the tension, initial deformation which started at the soft mesh regions continues to be localized around their original location; as the deformation continues, the deformation regions are still restricted to their original location despite more new deformed regions being created elsewhere, including those with larger free volumes. When localized regions have finally developed, the deformation bands do not look smooth and straight but are rather irregular and angular and have many side bands, which are coincident with the experimental results shown in Figure 20(b). The localized deformation zones are distributed more widely [21].

Figure 21 shows the SEM images of crack tips on HPT-treated (N=2) bulk metallic nanoglass and relatively homogeneous metallic glass before sample fracture. The HPT-treated bulk metallic nanoglass has numerous shear bands branching off and interacting with each other at the tip, which is not the case in the relatively homogeneous metallic glass. In the structure of the HPT-treated sample, the nanometer-scale glassy or crystalline second phase blocks and/or

blunts the propagation of the cracks. Stress is released by the formation of new shear bands. The propagation of the newly-formed shear bands is again inhibited by branching and intersection [51].

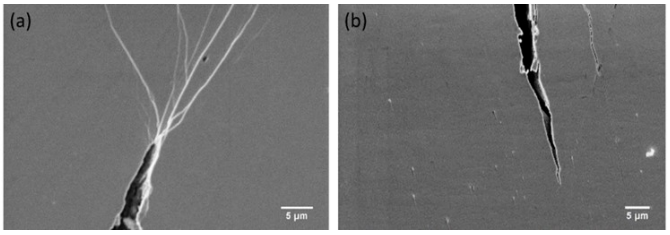

Figure 21. SEM images of crack tips during tensile tests on the HPT-treated (N=2) (a) $Zr_{55.7}Ni_{10}Al_7Cu_{19}Co_{8.3}$ bulk metallic nanoglass and (b) $Zr_{64}Ni_{10}Al_7Cu_{19}$ metallic glass [50]. (Reprinted from Ref. [50]. Copyright © 2019 Materials)

5. Thin film metallic nanoglasses synthesized by magnetron sputtering

Above three sections, we described three common techniques to fabricate bulk metallic nanoglasses. Here we introduce magnetron sputtering technique, which can prepare thin film metallic nanoglasses. Schematic illustration of magnetron sputtering is shown in Figure 22. A negative potential is applied to the target, acting as cathode. Electrons are repelled from the target. They collide with Ar atoms, forming Ar^+ ions. Ar^+ ions are then accelerated in the magnetic field and collision with the target. In this way, atoms in the target are ejected and deposit on the substrate.

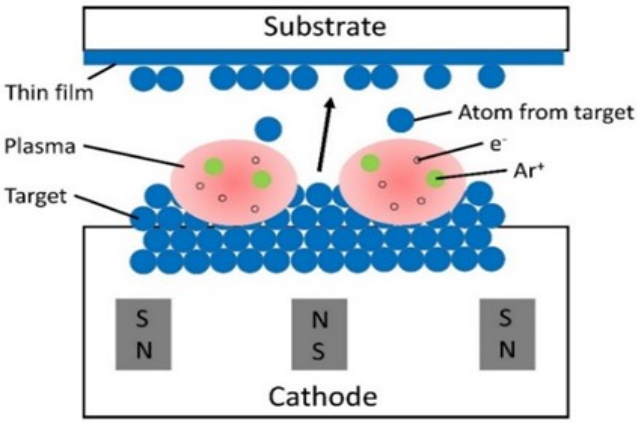

Figure 22. Schematic illustration of magnetron sputtering

Magnetron sputtered $Au_{40}Cu_{28}Pd_5Ag_7Si_{20}$ metallic glasses films were reported [52]. It is found that working pressure of Ar affects the films structure: homogeneous at low working pressures and nanostructured with mesoscopic hills and nanometer-sized-columns at higher working pressures, as shown in Figure 23 [52]. Clusters in sputtered Au-based nanoglass could have an average size of 30 nm. It is possible to derive a power law from the mean cluster size variation with deposition time, indicating that the growth of the glassy cluster is diffusion-controlled [53,54]. It is larger in Ti- based samples with a diameter of 100-300 nm. During this preparation, it has to be interrupted for 10 minutes after 10 minutes of continuous sputtering in order to prevent the significant heating of the substrate [55]. In addition, other parameters, e.g., deposition rate and substrate temperature, can also achieve nanostructured metallic glass films, which was recently reviewed [56].

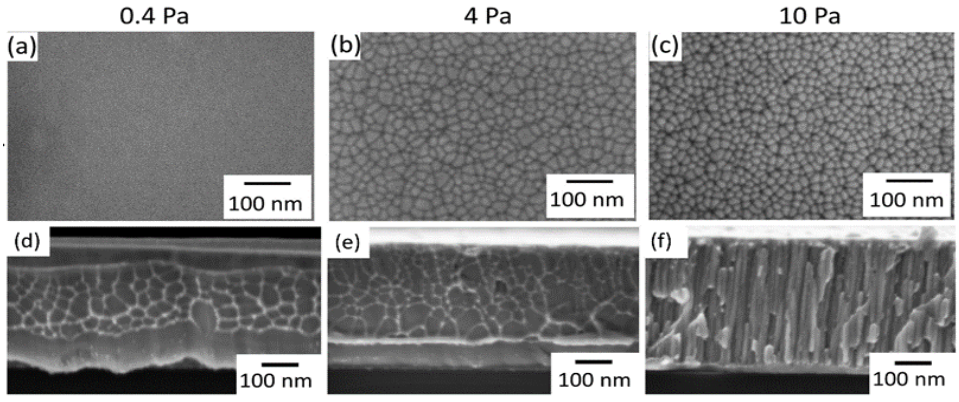

Figure 23. SEM images of the top view of $Au_{40}Cu_{28}Pd_5Ag_7Si_{20}$ thin films deposited on clean Si<100>at working pressures of Ar of (a) 0.4, (b) 4 and (c) 10 Pa and cross section at working pressures of (d) 0.4, (e) 4 and (f) 10 Pa [52]. (Reprinted from Ref. [52]. Copyright © 2018 Thin Solid Films)

6. Summary and outlook

Metallic nanoglass is metallic glass consisting of nanometer-sized glassy clusters and glass/glass interfaces. Their mechanical properties are improved as a result of the hard glassy clusters' inhibition effect on shear band sliding, and more numerous shear band initiation sites in the interfaces with enhanced free volume. Structure and properties of metallic nanoglasses can be further modified.

Various methods can be used to synthesize bulk metallic nanoglasses. Inert gas condensation-consolidation is the first method to have been developed. By carefully designing its composition, such as $Zr_{55.7}Ni_{10}Al_7Cu_{19}Co_{8.3}$, bulk metallic nanoglass can be obtained using phase separation in metallic glass. Compressive plasticity of the phase-separated bulk metallic nanoglass improves significantly compared with relatively homogeneous metallic glass. Shear bands have a similar structure to the glass/glass interfaces. So severe plastic deformation – such as HPT treatment – on particular metallic glasses is another possible method for synthesizing bulk metallic nanoglass. To do this, it is necessary to have a high number density of shear bands and different orientations to form network structure. Both hardening and toughening can be achieved by HPT-treated treatment (2 rotations) on bulk metallic nanoglass ($Zr_{55.7}Ni_{10}Al_7Cu_{19}Co_{8.3}$) with a tensile plastic strain of around 1%. All these bulk metallic nanoglass synthesis methods are still being developed. The knowledge obtained here for bulk metallic nanoglasses are also useful for conventional oxide nanoglasses. Because of the significantly improved mechanical properties, conventional oxide nanoglasses could also have large application potential. Energy consumption and CO_2 emission problems will be further investigated for industrial applications. Furthermore, nanoglasses are good precursors for the preparation of porous materials which can be used for biomaterials.

Acknowledgements

Financial supports from the National Key Research and Development Program of China (2016YFB0700201, 2016YFB0701203, and 2017YFA0403400), the National Natural Science Foundation of China (U1832203, 11975202, 51671170 and 51671169), the China Scholarship Council (Grant No. 201306120026), the Natural Science Foundation of Zhejiang Province (grants Z1110196, Y4110192 and LY15E010003), KNMF project (2016-015-010609), German Academic Exchange Service DAAD (STIBET Doktoranden), Deutsches Zentrum für Luft- und Raumfahrt e.V. (DLR ThermoLab VI 50 WM 1759) and the Fundamental Research Funds for the Central Universities are gratefully acknowledged.

REFERENCES

[1] C. Suryanarayana, A. Inoue, "Bulk Metallic Glasses," CRC Press, 2011. View Article

[2] H. Gleiter, "Our thoughts are ours, their ends none of our own: Are there ways to synthesize materials beyond the limitations of today?," Acta Materialia, vol. 56, pp. 5875-5893, 2008. View Article

[3] W.L. Johnson, "Bulk glass-forming metallic alloys: science and technology," MRS buL.lletin, vol. 24, no. 10, pp. 42-56, 1999. View Article

[4] A.L. Greer, E. Ma, "Bulk metallic glasses: at the cutting edge of metals research," MRS bulletin, vol. 32, no. 8, pp. 611-619, 2007. View Article

[5] H.J. Fecht, "Defect-induced melting and solid-state amorphization," Nature, vol. 356, pp. 133-135, 1992. View Article

[6] H.W. Sheng, W.K. Luo, F.M. Alamgir, J.M. Bai, E. Ma, "Atomic packing and short-to-medium-range order in metallic glasses," Nature, vol. 439, pp. 419-425, 2006. PMid:16437105 View Article PubMed/NCBI

[7] A.L. Greer, Y.Q. Cheng, E. Ma,"Shear bands in metallic glasses," Materials science and engineering R, vol. 74, pp. 71-132, 2013. View Article

[8] A.J. Cao, Y.Q. Cheng, E. Ma, "Structural processes that initiate shear localization in metallic glass," Acta Materialia, vol. 57, pp. 5146-5155, 2009. View Article

[9] M.F. Ashby, A.L. Greer, "Metallic glasses as structural materials," Scripta Materialia, vol. 54, no. 3, pp. 321-326, 2006. View Article

[10] A.R. Yavari, J.J. Lewandowski, J. Eckert, "Mechanical properties of bulk metallic glasses," MRS Bulletin, vol. 32, pp. 635-638, 2007. View Article

[11] H. Gleiter, "Nanoglasses: A new kind of noncrystalline material and the way to an age of new technologies?" Small, vol. 12, no. 16, pp. 2225-2233, 2016. PMid:26756322 View Article PubMed/NCBI

[12] J. Jing, A. Krämer, R. Birringer, H, Gleiter, U. Gonser, "Modified atom structure in a Pd70Fe3Si27 nanoglass: A Mössbauer study." Journal of Non-Crystalline Solids, vol. 113, pp. 167-170, 1989. 90007-0 View Article

[13] H. Gleiter, "Are there ways to synthesize materials

beyond the limits of today?" Metallurgical and Materials Transactions A, vol. 40, pp. 1499-1509, 2009. View Article

[14] O. Adjaoud, K. Albe, "Interfaces and interphases in nanoglasses: Surface segregation effects and their implications on structural properties," Acta Materialia, vol. 113, pp. 284-292, 2016. View Article

[15] Y. Ritter, D. Sopu, H. Gleiter, K. Albe, "Structure, stability and mechanical properties of internal interfaces in Cu64Zr36 nanoglasses studied by MD simulations," Acta Materialia, vol. 59, no. 17, pp. 6588-6593, 2011. View Article

[16] A. Stoesser, M. Ghafari, A. Kilmametov, H. Gleiter, Y. Sakurai, M. Itou, S. Kohara, H. Hahn, S. Kamali, "Influence of interface on structure and magnetic properties of Fe50B50 nanoglass," Applied Physics Letters, vol. 116, pp. 134305, 2014. View Article

[17] M. Ghafari, S. Kohara, H. Hahn, H. Gleiter, T. Feng, R. Witte, S. Kamali, "Structural investigations of interfaces in Fe90Sc10 nanoglasses using high-energy x -ray diffraction," Applied Physics Letters, vol. 100, pp. 133111, 2012. View Article

[18] H. Gleiter, "Nanoglasses: A new kind of noncrystalline materials," Beilstein Journal of Nanotechnology, vol. 4, pp. 517-533, 2013. PMid:24062978 View Article PubMed/NCBI

[19] H. Gleiter, T. Schimmel, H. Hahn, "Nanostructured solids - From nano-glasses to quantum transistors," Nano Today, vol. 9, pp. 17-68, 2014. View Article

[20] J.X. Fang, U. Vainio, W. Puff, R. Wurschum, X.L. Wang, D. Wang, M. Ghafari, F. Jiang, J. Sun, H. Hahn, H. Gleiter, "Atomic Structure and Structural Stability of Sc75Fe25 Nanoglasses, "Nano Letters, vol. 12, pp. 458-463, 2012. PMid:22122554 View Article PubMed/NCBI

[21] Y. Wang, M. Li, J. Xu, "Toughen and harden metallic glass through designing statistical heterogeneity," Scripta Materialia, vol. 113, pp. 10-13, 2016. View Article

[22] D. Sopu, K. Albe, Y. Ritter, H. Gleiter, "From nanoglasses to bulk massive glasses," Applied Physics Letters, vol. 94, pp. 191911, 2009. View Article

[23] R. Witte, T. Feng, J.X. Fang, A. Fischer, M. Ghafari, R. Kruk, R.A. Brand, D. Wang, H. Hahn, H. Gleiter, "Evidence for enhanced ferromagnetism in an iron-based nanoglass," Applied Physics Letters, vol. 103, pp. 073106, 2013. View Article

[24] D.H. Kim, W.T. Kim, E.S. Park, N. Mattern, J. Eckert, "Phase separation in metallic glasses," Progress in Materials Science, vol. 58, no. 8, pp. 1103-1172, 2013. View Article

[25] B.J. Park, H.J. Chang, D.H. Kim, W.T. Kim, K. Chattopadhyay, T.A. Abinandanan, S. Bhattacharyya, "Phase separating bulk metallic glass: a hierarchical composite," Physical Review Letters, vol. 96, pp. 245503, 2006. PMid:16907253 View Article PubMed/NCBI

[26] S.S. Chen, H.R. Zhang, I. Todd, "Phase-separation-enhanced plasticity in a Cu47.2Zr46.5Al5.5Nb0.8 bulk metallic glass," Scripta Materialia, vol. 72-73, pp. 47-50, 2014. View Article

[27] Y. Dong, R. Wunderlich, J. Biskupek, Q.P. Cao, X.D. Wang, D.X. Zhang, J.Z. Jiang, H.-J. Fecht. "Co content effect on elastic strain limit in ZrCuNiAlCo bulk metallic glasses," Scripta Materialia, vol. 137, pp. 94-99, 2017. View Article

[28] A. Takeuchi, A. Inoue, "Classification of bulk metallic glasses by atomic size difference, heat of mixing and period of the main alloying element," Materials Transactions, vol. 46, no. 12, pp. 2817-2829, 2005. View Article

[29] Q. Yu, X.D. Wang, H.B. Lou, Q.P. Cao, J.Z. Jiang, "Atomic packing in Fe-based metallic glasses," Acta Materialia, vol. 102, pp. 116-124, 2016. View Article

[30] C.C. Hays, C.P. Kim, W.L. Johnson, "Microstructure controlled shear band pattern formation and enhanced plasticity of bulk metallic glass containing in-situ formed ductile phase dendrite dispersions," Physical Review Letters, vol. 84, pp. 2901, 2000. PMid:11018971 View Article PubMed/NCBI

[31] H. Shao, Y. Xu, B. Shi, C. Yu, H. Hahn, H. Gleiter, J. Li, "High density of shear bands and enhanced free volume induced in Zr70Cu20Ni10 metallic glass by high-energy ball milling," Journal of Alloys and Compounds, vol. 548, pp. 77-81, 2013. View Article

[32] Y. Zhang, A.L. Greer, "Thickness of shear bands in metallic glasses," Applied Physics Letters, vol. 89, no. 7, pp. 071907, 2006. View Article

[33] M.Q. Jiang, W.H. Wang, L.H. Dai, "Prediction of shear-band thickness in metallic glasses," Scripta Materialia, vol. 60, no. 11, pp. 1004-1007, 2009. View Article

[34] Y.M. Chen, T. Ohkubo, T. Mukai, K. Hono, "Structure of shear bands in Pd40Ni40P20 bulk metallic glass," Journal of Materials Research, vol. 24, no. 1, pp. 1-9, 2011. View Article

[35] J.J. Lewandowski, A.L. Greer, "Temperature rise at shear bands in metallic glasses," Nature Materials, vol. 5, pp. 15, 2005. View Article

[36] N.P. Bailey, J. Schiøtz, K.W. Jacobsen, "Atomistic simulation study of the shear-band deformation mechanism in Mg-Cu metallic glasses," Physical Review B, vol. 73, no. 6, pp. 064108, 2006. View Article

[37] D. Klaumünzer, A. Lazarev, R. Maaß, F.H. Dalla Torre, A. Vinogradov, J.F. Löffler, "Probing shear-band initiation in metallic glasses," Physical Review Letters, vol. 107, no. 18, pp. 185502, 2011. PMid:22107642 View Article PubMed/NCBI

[38] J. Pan, Q. Chen, L. Liu, Y. Li, "Softening and dilatation in a single shear band," Acta Materialia, vol. 59, no. 13, pp. 5146-5158, 2011. View Article

[39] J. Bokeloh, S.V. Divinski, G. Reglitz, G. Wilde, "Tracer measurements of atomic diffusion inside shear bands of a bulk metallic glass," Physical Review Letters, vol. 107, no. 23, pp. 235503, 2011. PMid:22182099 View Article PubMed/NCBI

[40] W.J. Wright, T.C. Hufnagel, W.D. Nix, "Free volume coalescence and void formation in shear bands in metallic glass," Journal of Applied Physics, vol. 93, no. 3, pp. 1432-1437, 2003. View Article

[41] P.W. Bridgman, "Effect of high shearing stress com-

bined with highdrostatic pressure," Phsycal Reciew, vol. 48, pp. 825-847, 1935. View Article

[42] X.D. Wang, Q.P. Cao, J.Z. Jiang, H. Franz, J. Schroers, R.Z. Valiev, Y. Ivanisenko, H. Gleiter, H.J. Fecht, "Atomic-level structural modifications induced by severe plastic shear deformation in bulk metallic glasses," Scripta Materialia, vol. 64, pp. 81-84, 2011. View Article

[43] W. Dmowski, Y. Yokoyama, A. Chuang, Y. Ren, M. Umemoto, K. Tsuchiya, A. Inoue, T. Egami, "Structural rejuvenation in a bulk metallic glass induced by severe plastic deformation," Acta Materialia, vol. 58, pp. 429-438, 2010. View Article

[44] P. Denis, C.M. Meylan, C. Ebner, A.L. Greer, M. Zehetbauer, H.J. Fecht, "Rejuvenation decreases shear band sliding velocity in Pt-based metallic glasses," Materials Science & Engineering A, vol. 684, pp. 517-523, 2017. View Article

[45] S.H. Joo, D.H. Pi, A.D.H. Setyawan, H. Kato, M. Janecek, Y.C. Kim, S. Lee, H.S. Kim, "Work-hardening induced tensile ductility of bulk metallic glasses via high-pressure torsion," Scientific Reports, vol. 5, no. 9660, 2015. PMid:25905686 View Article PubMed/NCBI

[46] N. Adachi, Y. Todaka, Y. Yokoyama, M. Umemoto, "Cause of hardening and softening in the bulk glassy alloy Zr50Cu40Al10 after high pressure torsion," Materials Science & Engineering A, vol. 627, pp. 171-181, 2015. View Article

[47] S. Hobor, A. Revesz, P.J. Szabo, A.P. Zhilyae, V.K. Kis, J.L. Labar, Z. Kovacs, "High pressure torsion of amorphous Cu60Zr30Ti10 alloy," Journal of Applied Physics, vol. 104, pp. 033525, 2008. View Article

[48] R.Z. Valiev, D.V. Gunderov, A.P. Zhilyaev, A.G. Popov, V.G. Pushin, "Nanocrystallization induced by severe plastic deformation of amorphous alloys," Journal of Metastable and Nanocrystalline Materials, Vol. 22, pp. 21-26, 2004. View Article

[49] C. Ebner, B. Escher, C. Gammer, J. Eckert, S. Pauly, C. Rentenberger, "Structural and mechanical characterization of heterogeneities in a CuZr-based bulk metallic glass processed by high pressure torsion," Acta Materialia, vol. 160, pp. 147-157, 2018. View Article

[50] Y. Dong, S.Y. Liu, J. Biskupek, Q.P. Cao, X.D. Wang, J.Z. Jiang, R. Wunderlich and H.-J. Fecht, "Improved tensile ductility by severe plastic deformation for a nano-structured metallic glass," Materials, vol. 12, pp. 1611, 2019. PMid:31100842 View Article PubMed/NCBI

[51] S. Xie, E.P. George, "Hardness and shear band evolution in bulk metallic glasses after plastic deformation and annealing," Acta Materialia, vol. 56, no. 18, pp. 5202-5213, 2008. View Article

[52] P. Denis, S.Y. Liu, H.-J. Fecht, "Growth mode transition in Au-based thin film metallic glasses," Thin Solid Films, vol. 665, pp. 29-35, 2018. View Article

[53] N. Chen, R. Frank, N. Asao, D.V. Louzguine-Luzgin, P. Sharma, J.Q. Wang, G.Q. Xie, Y. Ishikawa, N. Hatakeyma, Y.C. Lin, M. Esashi, Y. Yamamoto, A. Inoue, "Formation and properties of Au-based nanograined metallic glasses," Acta Materialia, vol. 59, no. 16, pp. 6433-6440, 2011. View Article

[54] N. Chen, D.V. Louzguine-Luzgin, G.Q. Xie, P. Sharma, J.H. Perepezko, M. Esashi, A.R. Yavari, A. Inoue, "Structure investigation and mechanical properties of a representative of a new class of materials: nanograined metallic glasses," A Nanotechnology,vol. 24, pp. 045610, 2013. PMid:23299703 View Article PubMed/NCBI

[55] N. Chen, X. Shi, R. Witte, K.S. Nakayama, K. Ohmura, H. Wu, A. Takeuchi, H. Hahn, M. Esashi, H. Gleiter, A. Inoue, D.V. Louzguine, "A novel Ti-based nanoglass composite with submicron-nanometer-sized hierarchical structures to modulate osteoblast behaviors," Journal of Materials Chemistry B, vol. 1, pp. 2568-2574, 2013. View Article

[56] S.Y. Liu, Q.P. Cao, X.D. Wang, D.X. Zhang, J.Z. Jiang, "Metallic glassy thin films: perspective on mechanical, magnetic, biomedical, and optical properties," Advanced Engineering Materials, vol. 21, no. 7, pp. 1900046, 2019. View Article